IEEE Photonics Journal
An IEEE Photonics Society Publication

Open Access

Radiation Pattern Measurement in the Planar Coordinate

Volume 11, Number 6, December 2019

Chen Yang, *Member, IEEE*
Yi-hao Wang
Yi Wang
Zhao Ding
Jun Wen
Li-Feng Bian

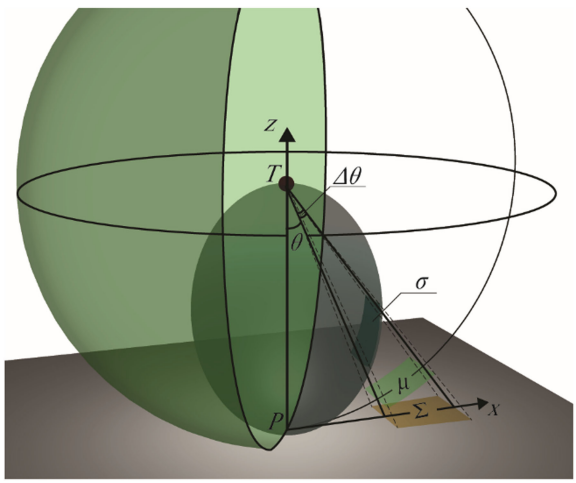

DOI: 10.1109/JPHOT.2019.2949147

IEEE photonics SOCIETY
IEEE

Radiation Pattern Measurement in the Planar Coordinate

Chen Yang,[1,2] ***Member, IEEE***, **Yi-hao Wang,**[1] **Yi Wang,**[1] **Zhao Ding,**[1] **Jun Wen,**[3] **and Li-Feng Bian**[4]

[1]College of Big Data and Information Engineering, Guizhou Key Laboratory of Micro-Nano-Electronics and Software Technology, Engineering Center of the Ministry of Education of Semiconductor Power Device Reliability, Guizhou University, Guiyang 550025, China
[2]Longmaster Information and Technology Co., Ltd., Guizhou 550081, China
[3]School of Computer and Electrical Information, Guangxi University, Nanning 530004, China
[4]Key Laboratory of Nanodevices and Applications, Suzhou Institute of Nano-Tech and Nano-Bionics Chinese Academy of Sciences, Suzhou 215123, China

DOI:10.1109/JPHOT.2019.2949147
This work is licensed under a Creative Commons Attribution 4.0 License. For more information, see https://creativecommons.org/licenses/by/4.0/

Manuscript received September 9, 2019; revised October 14, 2019; accepted October 18, 2019. Date of publication October 23, 2019; date of current version November 26, 2019. This work was supported in part by the National Natural Science Foundation of China under Grant 61604046, in part by Scientific Plan Projects of Guizhou Province under Grants 20175788 and 20185781, in part by Open Fund of the Semiconductor Power Device Reliability Ministry of Education Engineering Research Center under Grant 20176103, and in part by Fund of Key Laboratory of Nano devices and Applications, Suzhou Institute of Nano-Tech and Nano-Bionics under Grant 18ZS08. Corresponding author: Chen Yang (e-mail: eliot.c.yang@163.com).

Abstract: A planar measurement approach is presented to obtain the radiation pattern, by which rotation operations can be removed or reduced for a source with narrow and divergent viewing angle, respectively. The Étendue conservation is applied to derive the intensity distribution relationship between planar and spherical surfaces, which is further used for the radiation feature measurement on planar systems. As an indirect approach, sampling position distribution and measurement sensitivity is then discussed. Four application scenarios of the method are proposed and experimentally studied, including: 1D, 3D wireframe, pattern reconstruction for Monte Carlo ray-tracing planar data and 3D pattern estimation for luminaires. 1D radiation pattern obtained by classical goniophotometer method is employed as an evaluation standard, and experiments indicate that the results agree well between the two approaches. Therefore, the planar measurement can be applied as an alternative or supplementary method of the goniophotometer to test angle-dependent attributes of sources.

Index Terms: Radiation pattern, planar measurement, Étendue conservation.

1. Introduction

Radiation pattern is a significant tool to describe angular dependent strength for sources, such as light from luminaires or radio waves from antennas. The radiation behavior can both reflect intrinsic characteristics of sources and consequently has great influence to optimize system performance [1]–[3]. In applications such as antenna design, radiation pattern with a reconfigurable feature is essential to establish different communication links [4].

At present, a majority of studies to obtain the radiation pattern can be classified into theoretical simulation and experimental measurement. Theoretically, the angular distribution behavior can be

obtained by calculated or simulated models, which are based on intrinsic attributes or working principles for versatile types of sources. The finite-difference time-domain (FDTD) method based on Maxwell's equations can be applied to generate patterns for complex source structures like OLED/LED [5]. Solutions or approximation solutions for beam equations is also an approach to provide the far-field pattern [6]. Monte Carlo (MC) ray tracing is another method to simulate radiation pattern with high precision [7]. In classical experiments, methods to obtain radiation patterns are based goniophotometer (G.M.) which can be classified into 3 types [8]. Nevertheless, in any type of the G.M., rotation is essential to measuring angular intensity variation in the spherical coordinate system [9], [10], where the sources are typically sampled in equal angular steps [11], [12]. Generally, the light strength is measured sequentially step by step, but multi-channel detection can be employed to shorten the measurement process [13]. Furthermore, in order to obtain a 3D radiation pattern, the biaxial mechanical setup is commonly required to provide rotation in the range of 0° to 180° and 0° to 360° around the polar and the azimuthal angle, respectively [1].

A lot of efforts have been made to optimize the radiation pattern measurement methods. Due to advantages such as flexibility and processing time-efficiency, Charge-Coupled Device (CCD) cameras are employed to construct video-goniophotometers in applications such as bidirectional scattering distribution function measurement [14], [15]. A multipurpose automatic angular attribute measurement platform is developed with computer aided angular motion, stimulus generator, data acquisition and visualization [16]. Though the radiation pattern is a far-field attribute of sources and the far-field measurement is the most straightforward method, near-field goniophotometries are developed to capture luminance images for all directions by imaging luminance measurement devices. As no distance restriction, it is regarded as a cost down approach with compact structures [17], [18].

Here, an approach is proposed to measure the radiation pattern in planar coordinate system, which can remove or reduce the rotation operation, especially for sources with narrow viewing angles. To achieve this target, the Étendue conservation is applied to derive intensity distribution mapping relationship between the planar and spherical system. Subsequently, as an indirect measurement method, sampling position arrangement and measurement sensitivity are discussed. Finally, experiments are carried out about four proposed application scenarios of the method, including: 1D measurement, 2D wireframe pattern measurement, radiation pattern reconstruction based on planar data generated by MC ray-tracing, and 3D pattern estimation for luminaires.

2. Theoretical

2.1 Relationship by Étendue Conservation

To measure radiation pattern in planar system, intensity distribution relationship between planar and spherical surface should be first investigated, which can be derived as schematically shown in Fig. 1. To measure the emission pattern, let us start with the isotropic point source for simplicity. As intensity distribution is uniform across the whole spherical surface centered with the source, a reference point *P* can be defined on the target plane which is perpendicular to line *TP*. μ and Σ are infinitesimal cross-sections on spherical and planar surfaces intersecting with an oblique pyramid rays, which can be geometrically approximated by a rectangle and trapezoid respectively. The light propagates in the free space can be regarded as the lossless system, where the Étendue is conserved on both of the infinitesimal surfaces [19]. When the top angle of the pyramid ($\Delta\theta$) approaches 0, intensity distribution follows equation (1): [20]

$$\varphi_{\sum}(\theta) = \varphi_{\mu}\cos^3\theta. \tag{1}$$

In which, $\varphi_{\Sigma}(\theta)$ is the intensity on the target plane, φ_{μ} is the intensity on the spherical surface, and θ is the tilt angle.

When radiation pattern of the source under test differs from the ideal point source, intensity is no more uniform on spherical surface, but *P* can still be regarded as the distribution reference point. Referring to *P*, the radiation pattern can be described by the intensity distribution relationship

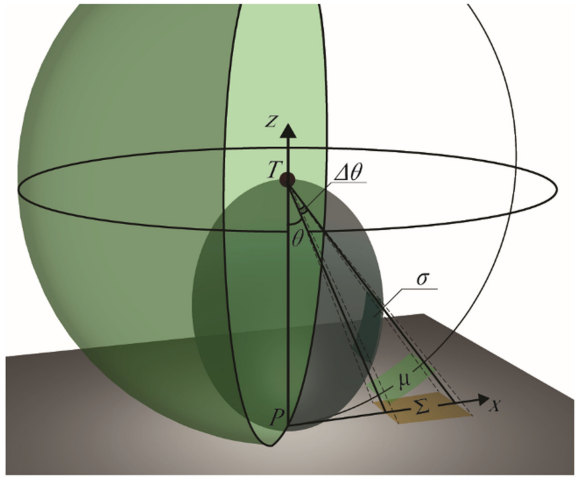

Fig. 1. Schematic of intensity distribution on different surfaces.

defined as follow,

$$\varphi_\sigma(\theta) = \varphi_p F(\theta). \tag{2}$$

Where, $\varphi_\sigma(\theta)$ is intensity at the θ angle direction of the source under test, φ_p is the intensity of reference P, and $F(\theta)$ is the attenuation factor in θ direction.

For ideal isotropic point source, the intensity φ_p across the whole spherical surface is constant and equals to the intensity at point P. Let $\varphi_p = \varphi_\mu$ and substitute equation (1) into (2),

$$\varphi_\sigma(\theta) = \varphi_\sum(\theta)F(\theta)\cos^{-3}\theta = \varphi_{\sum\theta}(\theta)\cos^{-3}\theta. \tag{3}$$

Where, $\varphi_{\Sigma\theta}(\theta)$ is the product of $\varphi_\Sigma(\theta)$ and $F(\theta)$, which represents intensity from the source under test at the direction θ of the target plane.

Equation (3) indicates intensity on spherical surface can be calculated from data on the planar surface at the same direction, which is proposed to measure radiation pattern in this paper. Since the radiation pattern is far field attribute of sources, it is usually measured on a spherical surface far enough away from devices under test. Therefore, like the far-field condition of conventional approaches, the distance between the source under test and the photodetector requires at least five times of the light output slot to ignore the influence of its size [21].

In order to apply the relationship in measurement, sampling positions on the plane need to be first calculated based on the preset measurement step. Then, intensity on these positions is measured and further mapped back to the spherical surface by the corresponding angle factor $\cos^{-3}\theta$ term.

2.2 Sampling Position Arrangement

According to Equation (3), θ is necessary to create mapping relationship between planar and spherical surface. In practical applications, arrangement of the sample positions can be arranged by two strategies: equal spatial interval step at a planar system or equal angle step at a spherical system.

Firstly, intensity measured with an equal spatial interval in a planar system is the most straightforward arrangement. In this case, θ can be calculated according to equation (4)

$$\theta = \arctan\left(\frac{\sqrt{x^2 + y^2}}{d}\right). \tag{4}$$

Where, (x, y) is coordinate of the sampling position at the plane, d is the distance from source to the plane. For 1D measurement, let $y = 0$ in equation (4), and then difference value of the two

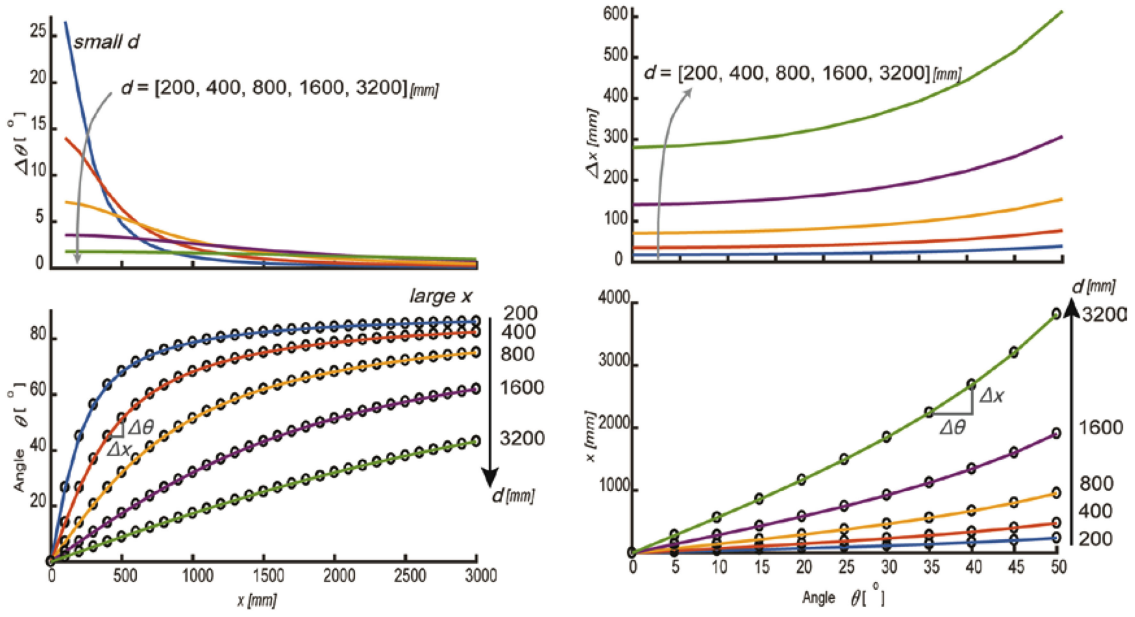

Fig. 2. Arrangement of sampling positions: (a) angular interval varies at equal spatial intervals and (b) spatial interval varies at equal angular intervals.

adjacent angles can be calculated by equation (5).

$$\Delta\theta = \arctan\left(\frac{x+\Delta x}{d}\right) - \arctan\left(\frac{x}{d}\right) = \arctan\frac{\Delta x/d}{1+x(x+\Delta x)/d^2} \tag{5}$$

In the equal Δx interval measurement, two position arranging schemes need to be avoided as it can be seen in Fig. 2(a) which is drawn based on Equation (4) and (5). First, when the sampling distance d is not large enough comparing to Δx and x, $\Delta\theta$ tends to distributed unevenly. Thus, the sampling step of the spherical coordinate have sparser interval in the region and more details would be lost around small θ region. Second, the sampling position x is so large that θ and $\Delta\theta$ approaches 90° and 0°, respectively. Further increase of the value x will cause sampling positions cluster in the spherical system, which cannot provide effective information.

When the sampling distance d is far greater than the sampling interval and position, equal spatial interval measurement can provide to a reasonable distribution in spherical system. Therefore, it is preferable to arrange the detector at far field without too board viewing angle when applying the planar measurement approach.

Secondly, for an equal angular interval measurement, equation (6) can be employed to calculate the coordinate of the sampling position.

$$x = d\tan\theta\cos\varphi,\ \ y = d\tan\theta\sin\varphi \tag{6}$$

Where, θ and φ are polar and the azimuthal angle, respectively.

Taken 1D measurement as the example for discussion simplification, let $\varphi = 0$ in equation (6), and the distance between two sampling points at the plane is indicated by equation (7):

$$\Delta x = d\tan(\theta+\Delta\theta) - d\tan\theta = d\frac{\sin\Delta\theta}{\cos(\theta+\Delta\theta)\cos\theta} \tag{7}$$

Fig. 2(b) is drawn based on equation (6) and (7) and it illustrates that sampling position design in equal $\Delta\theta$ measurement must consider to limit the scope of sampling distance d and viewing angle

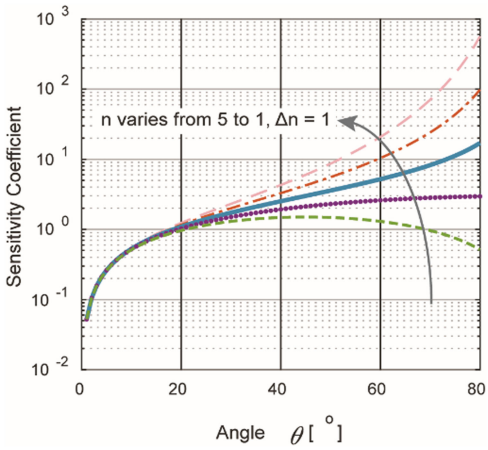

Fig. 3. Measurement sensitivity coefficient varies with θ.

θ, both resulting in a large spatial requirement. An extreme case is that angle θ is equal to or greater than 90°, the sampling position will be outside the planar range.

Since the distance is no longer a constant in the planar coordinate and the intensity of light from sources varies inversely as the square of the distance, it requires a much higher range for the sensor, which is one of the reasons not to arrange the sampling positions at large viewing angles.

2.3 Measurement Sensitivity

Measurement sensitivity caused by angle error is another factor must be considered during sampling. Based on equation (3),

$$\delta\varphi_\sigma = \left|\frac{\partial\varphi_\sigma}{\partial\theta}\right|\delta\theta = [3\varphi_{\sum\theta}(\theta)\cos^{-3}\theta\tan\theta]\delta\theta. \tag{8}$$

Thus, the sensitive coefficient due to angle θ is determined by $3\varphi_{\Sigma\theta}(\theta)\cos^{-3}\theta\tan\theta$.

Equation (8) indicates that both θ and the attribute of the source have impact on the measurement sensitivity. Let us assume that the intensity distribution on the plane is described by equation (9) for the sake of simplicity [22].

$$\varphi_{\sum\theta} = \varphi_p\cos^n\theta. \tag{9}$$

As detailed in equation (1), the intensity distributed on a plane emitted from an ideal point source follows the cubic cosine rule on the plane, that is to say, n equals to 3 in equation (5). When $n < 3$, intensity attenuates faster than the isotropic source when θ increases. However, if $n > 3$, the intensity on the plane increases with θ with respect to point P, such as the bat-wing style distribution shown in Fig. 7. Fig. 3 illustrates that the sensitivity coefficient varies as a function of angle θ. For sources with large n, the measurement becomes more sensitive at a large θ angle value. Otherwise, θ has less impact on the sensitivity, but high sensitive detector is required to react to the low light power due to long distance. Therefore, although not compulsory, it is preferable to distribute the sampling positions around the point with strongest light intensity, and arrange the angular scope according to the measurement requirement.

3. Experiment and Results

3.1 1D Measurement

Fig. 4 indicates experiments for a LED by the planar and the G.M. approach. The experiment setup is easy to implement as demonstrated in Fig. 4(a), in which the aperture array is preset in an equal

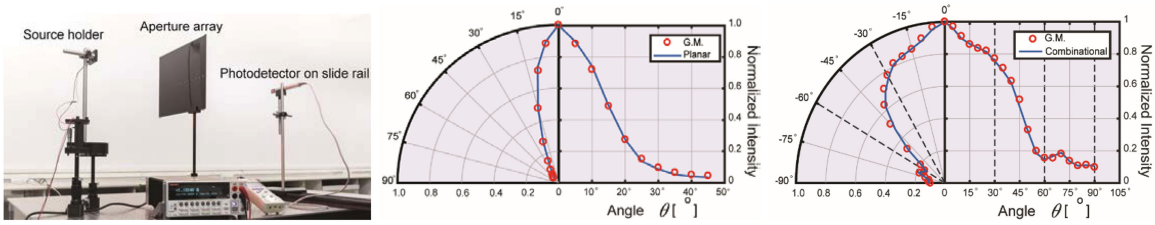

(a) (b) (c)

Fig. 4. Radiation patterns for LEDs: (a) experiment setup, (b) a collimated LED, and (c) a wide view LED by the combinational method with 30° in each group.

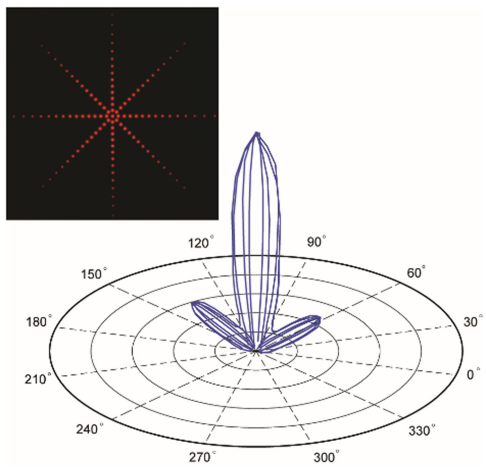

Fig. 5. 3D wireframe radiation pattern of a luminaire by the combinational method. Inset: Sample points distribution on the plane.

angular interval arrangement according to equation (6) to determine the sampling position. Fig. 4(b) is performed at an equal angular sampling with a step size of 5°, ranging from 0° to 45°.

As in the measurement process, systematic and random errors are inevitable, which arouse from different measurement setups, system disturbance, environmental changes, instrument drift, observation, electrical noise and so on [23]. The root mean square error (*RMSE*) is widely applied to evaluate the result agreement between two approaches, which is easy to be computed and has straightforward meaning of representing the normalized distance of the two datasets [24]. The *RMSE* indicated in Fig. 4(b) between the proposed and conventional methods is 0.0059.

To extend application of the proposed method, it can be combined with rotation for large view sources. By dividing the sampling process into groups, the rotation operation is performed between different groups, and removed in the same group by using the mapping equation (3). Fig. 4(c) shows the combinational measurement of a large view LED, ranging from 0° to 90°, with 30° in each group. The *RMSE* between the combinational measurement and G.M. methods is 0.0071.

The experimental results demonstrate that the values obtained by the proposed relationship agree well with the conventional method. Therefore, the planar approach can be applied as a candidate to measure the radiation pattern without rotation for narrow beam sources.

3.2 3D Wireframe Measurement

Due to the well agreement, 3D wireframe radiation pattern can be obtained by the proposed approach to provide designers with the overall properties of complex sources, which is hard to be represented by 1D patterns. Fig. 5 is an example of 3D wireframe radiation pattern for a luminaire with 3 emission lobes. It is an equal angular step measurement which shares the setup as in

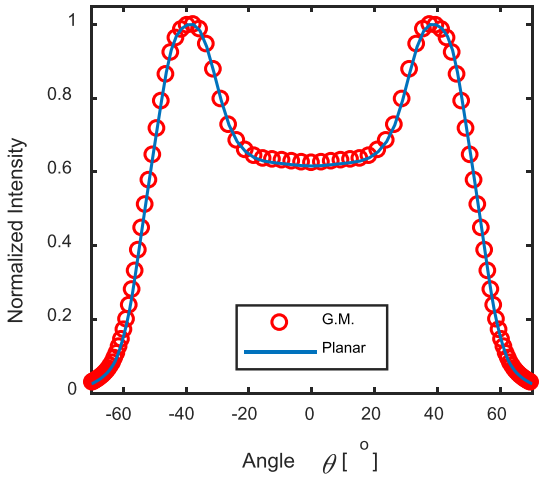

Fig. 6. Radiation pattern for a bat-wing LED by MC ray tracing simulation.

Fig. 4(a) except the aperture array is firstly set based on equation (6) as demonstrated in insets of Fig. 5. Secondly, the source is collimated to the test plane and its intensity is subsequently measured at the positions. Next, rotate the source and repeat the steps until all concerned regions have been measured. Then, equation (3) is applied to map intensity from the planar surface back to spherical surface. Finally, results are combined together with rotation operators.

3.3 Pattern Reconstruction for Monte Carlo Ray Tracing Data

The MC ray tracing technique is a widely used simulation algorithm in applications such as image, nonimage system design, computer graphic rendering and so on. Due to advantages such as easy-to-implement, fit-for-parallel computation and high accuracy, it is usually as a gold standard to evaluate other algorithms [25]. In view of where the rays are emitted, MC ray tracing can be classified forward or backward one. The forward one simulates the physical rule of rays which emit from source, propagate through light path and finally reach detectors. It can provide more complete results for all preset detectors, but it is usually time costive and requires several hours or days to render a complex scenario. The backward one traces rays back from detectors to the source, in which increasing the number detectors will increase the computational burden. To obtain the radiation pattern by MC ray tracing commonly needs additional program codes for the function, or depends on whether the function is provided by a simulation tool. Even though the radiation pattern can be analyzed by tools, a large number of rays are sometimes required [26], which results in additional computation time and resource. Once the radiation pattern analysis is not scheduled during simulation, it is inevitable to repeat the previous time consuming process.

Fig. 6 is an example of bat-wing emitting LED by MC ray tracing algorithm ranging from $-60°$ to $60°$. The simulation compares results between direct spherical data and planar data mapped according to equation (3), which is an equal spatial step measurement. Under the simulation condition, the *RMSE* between the two methods is 0.0052. It indicates that the mapping relationship provides a high accurate method to reconstruct the radiation pattern at a much lower cost, by which extra spherical detector, re-simulation process or even the radiation pattern analysis function of a tool are not essential for view limited sources.

Equation (3) can also help to reconstruct the 3D pattern from the 2D meshed plane which is generally used as illumination sensors in MC ray-tracing. Fig. 7 demonstrates the recovered 3D radiation patterns based on the relationship for three energy limit patterns, including Gaussian, Laguerre–Gaussian beam [27] and Ince–Gaussian [28]. It can be seen that the meshed detector provides the equal spatial interval sampling at Cartesian coordinate, such that the mesh blocks

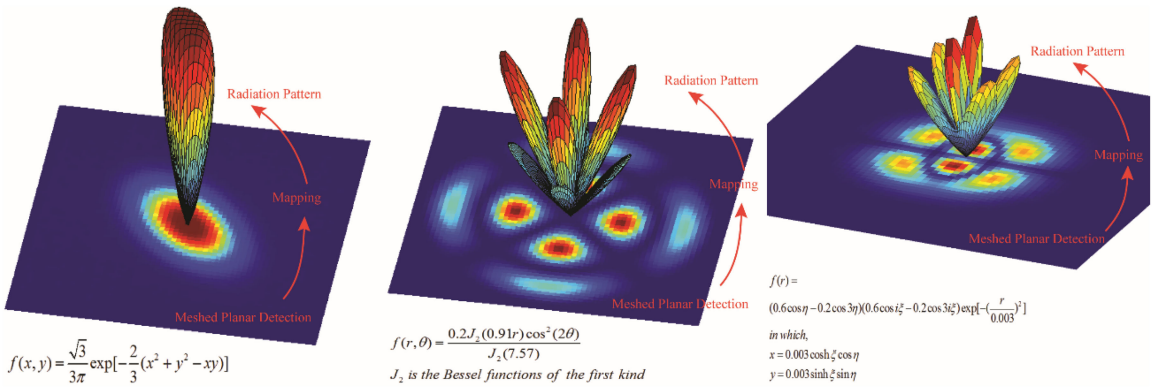

Fig. 7. 3D radiation pattern reconstructed from 2D data.

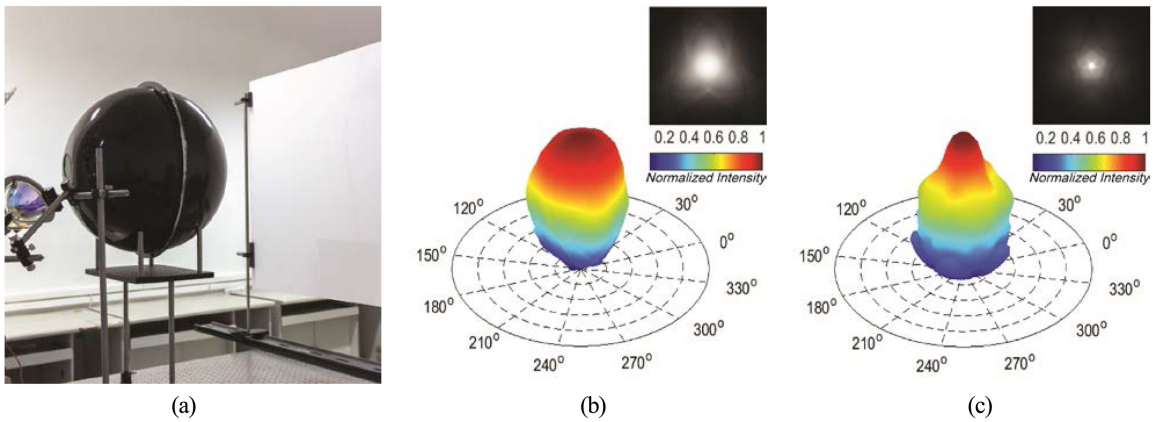

Fig. 8. 3D radiation pattern estimation for luminaires: (a) experiment setup, (b) ellipsoid-spherical combined structure [33], and (c) dodecahedron solar simulator [20]. Insets: 2D distribution captured on planar screen.

twist from squares into closed regions with curved edges of varying areas. In each block of the mesh, intensity is a constant which represents the average value in the region.

3.4 3D Pattern Estimation for luminaires

Volumetric rather than compact luminaires are commonly used in applications such as solar simulator, medical systems, and so on. To obtain the radiation pattern of luminaires with G.M., large components are necessary to rotate the luminaire, or large testing room space is required to rotate of the detectors [29]. Thus, it is costive to estimate the 3D radiation pattern for large luminaires [30]. However, the 2D pattern is more easily to be captured on planar surface through screens or directly by CCD [31], [32], thus equation (3) can provide a basic morphology of the radiation pattern for estimation.

Fig. 8 illustrates two estimated 3D radiation pattern of two energy limited luminaires, which is mapping back from 2D planar pattern captured through the screen as demonstrated in Fig. 8(a). In particular, Fig. 8(b) is a combined source structure with separated components [33], for which it is difficult to keep relative spatial position during rotation. In this case, the mapping relationship provides designers with a rapid and convenient approach to preliminarily estimate the radiation pattern shape.

4. Conclusion

In conclusion, the $\cos^{-3}\theta$ term representing the intensity relationship between planar to spherical surfaces is derived according to the Étendue conservation, which is further recommended for measuring radiation patterns in the planar coordinate. By using the relationship, intensity on the testing plane and the angle θ needs to be measured first. Subsequently, sampling position plan and measurement sensitivity is discussed, which suggests that the proposed method can be applied for narrow beam sources without rotation and extended for large view sources when combined with rotations.

Four application scenarios are presented based on the relationship and then studied by experiments. First, the 1D measurement of a narrow beam LED shows that the *RMSE* between the proposed and G.M. approach is 0.0059, while the *RMSE* is 0.0071 when measuring a wide view LED by three rotating groups, which indicates that the proposed strategy has high agreement with the G.M. Accordingly, the 3D wireframe pattern for a more complex source is obtained by mapping 2D plane data and then combined together with rotation operators. Furthermore, MC ray tracing results of 1D LED radiation patterns illustrates that the *RMSE* between the two methods is 0.0052, which indicates the relationship can maintain high precision in simulation applications. Thus, it is further employed to reconstruct 3D radiation patterns from simulated intensity distribution on 2D mesh detectors at a low cost. Finally, the relationship is proposed to rapid estimate the basic morphology of 3D radiation pattern for volumetric luminaires, which is constructed based on intensity captured by a screen or CCD. Experiments are performed to estimate 3D patterns for an ellipsoid-spherical combined luminaire and a dodecahedron illumination solar simulator.

Therefore, the proposed method is easy to implement and has a high consistency with conventional one in narrow beam source measurements. It also provides a swift way to estimate the basic shape of 3D radiation pattern according to 2D intensity distribution. Furthermore, it is easier to integrate multiple detectors on a plane than on a spherical surface, which allows multichannel systems (distributed such as the inset of Fig. 6) to be designed at a low cost in future works to speed up the data acquisition process. Although measurement scope by the approach should be limited due to sensitivity and space requirements, it can be combined with rotation setups to extend its applications and works as a supplementary method of G.M. to obtain radiation patterns without or with less rotation operations.

References

[1] H. J. Chen and Z. Y. Xu, "OLED panel radiation pattern and its impact on VLC channel characteristics," *IEEE Photon. J.*, vol. 10, no. 2, Apr. 2018, Art. no. 7901410.
[2] J. Ding, C. I, and Z. Xu, "Indoor optical wireless channel characteristics with distinct source radiation patterns," *IEEE Photon. J.*, vol. 8, no. 1, Feb. 2016, Art. no. 7900115.
[3] C. Wiesmann, K. Bergenek, R. Houdre, R. P. Stanley, N. Linder, and U. T. Schwarz, "Theoretical investigation of the radiation pattern from leds incorporating shallow photonic crystals," *IEEE J. Quantum Electron.*, vol. 45, no. 10, pp. 1273–1283, Oct. 2009.
[4] S. Yan and G. A. E. Vandenbosch, "Radiation pattern-reconfigurable wearable antenna based on metamaterial structure," *IEEE Antennas Wireless Propag. Lett.*, vol. 15, pp. 1715–1718, Feb. 2016.
[5] Y. H. Hsiao *et al.*, "Light extraction enhancement with radiation pattern shaping of LEDs by waveguiding nanorods with impedance-matching tips," *Nanoscale*, vol. 6, no. 5, pp. 2624–2628, 2014.
[6] S. R. Seshadri, "Radiation pattern of cylindrically symmetric scalar Laguerre–Gauss beams," *Opt. Lett.*, vol. 32, pp. 1159–1161, 2007.
[7] R. Hu, X. B. Luo, H. Feng, and S. Liu, "Effect of phosphor settling on the optical performance of phosphor-converted white light-emitting diode," *J. Lumin.*, vol. 132, pp. 1252–1256, 2012.
[8] International Commission on Illumination, *The Measurement of Absolute Luminous Intensity Distributions*. Vienna, Austria: Central Bureau CIE, 1987.
[9] J. V. Rudd, J. L. Johnson, and D. M. Mittleman, "Quadrupole radiation from terahertz dipole antennas," *Opt. Lett.*, vol. 25, pp. 1556–1558, 2000.
[10] Q. Xu *et al.*, "3-D antenna radiation pattern reconstruction in a reverberation chamber using spherical wave decomposition," *IEEE Trans Antennas Propag.*, vol. 65, no. 4, pp. 1728–1739, Apr. 2017.
[11] B. Krummacher, M. Klein, N. V. Malm, and A. Winnacker, "Optical analysis of down-conversion OLEDs," *Proc. SPIE*, vol. 6910, pp. 691007-1–691007-17, 2008.

[12] A. Kadiyala, K. Lee, L. E. Rodak, L. A. Hornak, D. Korakakis, and J. M. Dawson, "Improvement in the light extraction of blue InGaN/GaN-based LEDs using patterned metal contacts," vol. 2, no. 2, pp. 16–22, Mar. 2014.
[13] P. M. Krenz, B. A. Lail, and G. D. Boreman, "Calibration of lead-line response contribution in measured radiation patterns of IR dipole arrays," *IEEE J. Sel. Topics Quantum Electron.*, vol. 17, no. 1, pp. 218–221, Jan./Feb. 2011.
[14] M. Andersen, E. Stokes, N. Gayeski, and C. Browne, "Using digital imaging to assess spectral solar-optical properties of complex fenestration materials: A new approach in video-goniophotometry," *Solar Energy*, vol. 84, pp. 549–562, 2010.
[15] M. Andersen, C. Roecker, and J. L. Scartezzini, "Design of a time-efficient video-goniophotometer combining bidirectional functions assessment for transmission and reflection," *Solar Energy Mater. Solar Cells*, vol. 88, pp. 97–118, 2005.
[16] M. Presso, S. R. Rossi, and C. M. Posse, "A platform for multipurpose goniometric measurements," in *Proc. IEEE Int. Instrum. Meas. Technol. Conf. Proc.*, Montevideo, Uruguay, 2014, pp. 1026–1030.
[17] M. López, K. Bredemeier, N. Rohrbeck, C. Véron, F. Schmidt, and A. Sperling, "LED near-field goniophotometer at PTB, " *Metrologia*, vol. 49, pp. S141–S145, 2012.
[18] J. Audenaert, R. P. C. Acuna, P. Hanselaer, and F. B. Leloup, "Practical limitations of near-field goniophotometer measurements imposed by a dynamic range mismatch," *Opt. Express*, vol. 23, pp. 2240–2251, 2015.
[19] R. J. Anderson, *Illumination Engineering: Design With Nonimaging Optics*, Hoboken, NJ, USA: Wiley, 2013, ch. 2.
[20] C. Yang, J. Wang, X. Guo, Y. Wang, and Z. Ding, "A multisource regular dodecahedron solar simulator structure for uniform flux," *IEEE J. Photovolt.*, vol. 6, no. 2, pp. 516–521, Mar. 2016.
[21] D. L. DiLaura, K. W. Houser, R. G. Mistrick, and G. R. Steffy, *The Lighting Handbook: Reference and Application*, New York, NY, USA: Illum. Eng. Soc. North Amer., 2001, ch. 10.
[22] S. J. Lee, "Analysis of light-emitting diodes by Monte Carlo photon simulation," *Appl. Opt.*, vol. 40, pp. 1427–1437, 2001.
[23] A. S. Morris and R. Langari, *Measurement and Instrumentation Theory and Application*, New York, NY, USA: Academic, 2016, ch. 3.
[24] Q. Weng, "Quantifying uncertainty of digital elevation models derived from topographic maps," in *Proc. Advances Spatial Data Handling*, Berlin, Germany, 2002, pp. 403–418.
[25] R. Yao, X. Intes, and Q. Fang, "Generalized mesh-based Monte Carlo for wide-field illumination and detection via mesh retessellation," *Biomed. Opt. Express*, vol. 7, pp. 171–184, 2016.
[26] S. Leyre *et al.*, "A hybrid tool for spectral ray tracing simulations of luminescent cascade systems" *Opt. Express*, vol. 22, pp. 24582–24593, 2014.
[27] A. A. Tovar, "Propagation of Laguerre–Bessel–Gaussian beams," *J. Opt. Soc. Amer. A*, vol. 17, pp. 2010–2018, 2000.
[28] M. A. Bandres and J. C. Gutiérrez-Vega, "Ince-Gaussian beams," *Opt. Lett.*, vol. 29, pp. 144–146, 2014.
[29] V. F. Muñoz-Martínez, J. Serón-Barba, R. Molina-Mesa, J. M. Gómez-de-Gabriel, J. Fernández-Lozano, and A. García-Cerezo, "Double reflection goniophotometer," *Metrologia*, vol. 43, no. 3, pp. 185–194, Feb. 2006.
[30] S. Yan and G. A. E. Vandenbosch, "Low-profile dual-band pattern diversity patch antenna based on composite right/left-handed transmission line," *IEEE Trans. Antennas Propag.*, vol. 65, no. 6, pp. 2808–2815, Jun. 2017.
[31] K. Mishchik, Y. Petit, E. Brasselet, A. Royon, T. Cardinal, and L. Canioni, "Patterning linear and nonlinear optical properties of photosensitive glasses by femtosecond structured light," *Opt. Lett.*, vol. 40, pp. 201–204, 2015.
[32] K. Sueda, G. Miyaji, N. Miyanaga, and M. Nakatsuka, "Laguerre-Gaussian beam generated with a multilevel spiral phase plate for high intensity laser pulses," *Opt. Express*, vol. 12, pp. 3548–3553, 2004.
[33] R. M. Zeng *et al.*, "Design of ellipsoid and spherical combined light source for uniform flux and color mixing," *IEEE Photon. J.*, vol. 11, no. 4, Aug. 2019, Art. no. 6500710.